A NOVEL APPROACH TO NEURITE TRACING IN FLUORESCENCE MICROSCOPY IMAGES

Erik Meijering
Erasmus MC—University Medical Center Rotterdam
Departments of Medical Informatics and Radiology
P.O. Box 1738, NL-3000DR Rotterdam, The Netherlands
Email: meijering@imagescience.org

Mathews Jacob
Swiss Federal Institute of Technology Lausanne
Institute for Biomedical Imaging, Optics, and Engineering
EPFL-STI-BIOE-LIB, BM-Ecublens, CH-1015 Lausanne, Switzerland
Email: mathews.jacob@epfl.ch

J.-C. Floyd Sarria
Swiss Federal Institute of Technology Lausanne, Institute of Neurosciences
EPFL-SV-INS-LNC, AI-Ecublens, CH-1015 Lausanne, Switzerland
Email: juan-carlos.sarria@epfl.ch

Michael Unser
Swiss Federal Institute of Technology Lausanne
Institute for Biomedical Imaging, Optics, and Engineering
EPFL-STI-BIOE-LIB, BM-Ecublens, CH-1015 Lausanne, Switzerland
Email: michael.unser@epfl.ch

ABSTRACT
In this paper we propose a new, interactive technique for the segmentation of elongated structures in images. It is based on the so-called live-wire segmentation paradigm and uses a newly developed steerable filter for computing local ridge strength and orientation. We describe the principles of our segmentation technique and present the results of preliminary experiments demonstrating its potential for the tracing of neurites in fluorescence microscopy images.

KEY WORDS
Biomedical imaging, image segmentation, neurite tracing, fluorescence microscopy.

1 Introduction

Segmentation of elongated structures is a key problem in several image processing and analysis applications. Examples include the detection of roads and valleys in satellite images [1], the extraction of blood vessels from retinal [2], magnetic resonance [3, 4], computed tomography [5, 6], or X-ray angiography [7] images for the purpose of quantification or visualization, and the tracing of neurons in three-dimensional (3D) confocal microscopy images for histological studies [8, 9].

In cellular biology the problem arises, for example, when studying the axonal and dendritic outgrowth of cortical neurons under influence of different promoting and inhibiting factors [10–13]. Since a cell in culture grows approximately in a single cell layer, these processes are usually studied by means of fluorescence microscopy. In contrast with confocal microscopy, this imaging modality results in two-dimensional (2D) images. While effective in showing a cell's outgrowth in its entirety, the images frequently contain ambiguities regarding the branching or crossing of neurites and the linking of fragmented neurite segments. Such deficiencies make it virtually impossible to develop fully automatic tracing techniques for this purpose. This is why, to date, biologists have resorted to manual delineation—a very time consuming process resulting in highly operator-dependent segmentations.

In this paper we propose a new, semiautomatic tracing technique that exploits the expertise of the biologist in removing ambiguities, but that greatly improves the accuracy and reproducibility and reduces the burden of delineating more clearly visible neurite segments. The technique is based on the live-wire segmentation paradigm [14–17], which we have tailored to the tracing of elongated image structures. To this end we have developed a new steerable filter for ridge detection, as well as a new function for translating local ridge strengths and orientations into costs maps, as required by the graph-searching algorithm involved in live-wire segmentation. We describe the principles underlying our interactive tracing technique and show the results of preliminary experiments demonstrating its potential for the mentioned application.

In *IASTED International Conference on Signal and Image Processing – SIP 2003*, in press.

2 Ridge Detector

In gray-level landscape representations of images, elongated structures manifest themselves as ridges. First-order differential operators are inadequate for detecting this type of structures, since they result in a double response in the transversal direction, whereas a single response is desirable. This suggests the use of second-order operators.

A frequently-used example of such an operator is the second-order directional derivative of the Gaussian kernel, $(\mathbf{r} \cdot \nabla)^2 G$, with $\mathbf{r}$ the normalized direction vector and G the Gaussian kernel. This operator can also be expressed in terms of $\mathbf{H}_G$, the Hessian of G, as

$$\mathbf{r}^T \cdot \mathbf{H}_G \cdot \mathbf{r}, \tag{1}$$

and is a steerable filter [18]. The local principal ridge directions at any point in an image f are those $\mathbf{r}$ for which the application of (1) yields a maximum and a minimum response, respectively. These directions are given directly by the eigenvectors of $\mathbf{H}_{f*G}$, the Hessian of the Gaussian-smoothed version of the image. Due to the symmetry of this matrix, these eigenvectors are orthogonal, with the eigenvector corresponding to the smaller absolute eigenvalue pointing in the longitudinal direction of the structure. Comparison of the eigenvalue magnitudes thus allows for discrimination between elongated versus non-elongated image structures—a fact that has recently been exploited for vessel analysis in angiography [3–5].

We now propose to modify the filter so as to make it even more sensitive to elongated image structures. Specifically, we propose to increase its flatness in the longitudinal direction near the origin. To this end we add to the original filter an α-fraction of the second-order derivative in the direction orthogonal to $\mathbf{r}$. This leads to the filter $\{(\mathbf{r} \cdot \nabla)^2 + \alpha(\mathbf{r}_\perp \cdot \nabla)^2\}G$, or

$$\mathbf{r}^T \cdot \mathbf{H}'_G \cdot \mathbf{r}, \tag{2}$$

where $\mathbf{H}'_G = \mathbf{H}_G + \alpha \mathbf{R}^T_{\pi/2} \mathbf{H}_G \mathbf{R}_{\pi/2}$, with $\mathbf{R}_\theta$ denoting the matrix representing a rotation with angle θ. For the relation between the eigenvectors $\mathbf{v}'_i$ and $\mathbf{v}_i$, and the eigenvalues λ'_i and λ_i, of $\mathbf{H}'_G$ versus $\mathbf{H}_G$, we find

$$\begin{cases} \mathbf{v}'_1 = \mathbf{v}_1, \\ \mathbf{v}'_2 = \mathbf{v}_2, \end{cases} \quad \text{and} \quad \begin{cases} \lambda'_1 = \lambda_1 + \alpha\lambda_2, \\ \lambda'_2 = \lambda_2 + \alpha\lambda_1, \end{cases} \tag{3}$$

which shows that the orientation of (2) is the same as that of (1). The desired improvement in sensitivity can be translated into the flatness criterion

$$\lim_{\mathbf{x} \to \mathbf{0}} (\mathbf{r}_\perp \cdot \nabla)^2 \left(\mathbf{r}^T \cdot \mathbf{H}'_G \cdot \mathbf{r}\right)(\mathbf{x}) = 0. \tag{4}$$

Since the left-hand side is equal to $(1 + 3\alpha)\|\mathbf{r}\|^4/\sigma^4$, with σ the standard deviation of the Gaussian kernel, it follows that the optimal value for the free parameter is $\alpha = -1/3$. Working out the details, it follows that both (1) and (2) are linear combinations of G_{xx}, G_{xy}, and G_{yy}, which implies that they have practically the same computational cost. A visual comparison of the shapes of the filters (1) and (2) is provided in Figure 1.

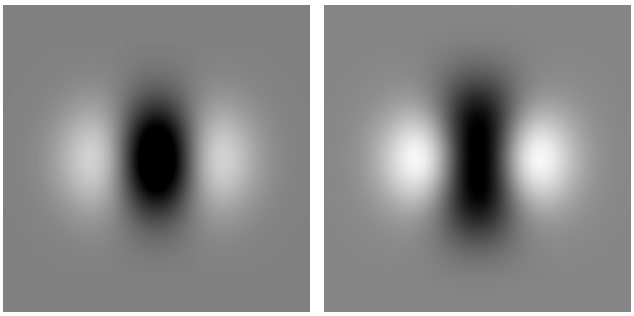

Figure 1. Impression of the shapes of the filters $\mathbf{r}^T \cdot \mathbf{H}_G \cdot \mathbf{r}$ (left) and $\mathbf{r}^T \cdot \mathbf{H}'_G \cdot \mathbf{r}$ (right), in this case with $\mathbf{r} = (1, 0)^T$. Clearly, the latter filter is more elongated and therefore more sensitive to ridge-like image structures.

As a measure of "ridgeness" we could now simply take the largest absolute eigenvalue of $\mathbf{H}'_{f*G}$, which we denote by $|\lambda'_1|$. In our application, however, we are interested only in bright ridges on a dark background, for which $\lambda'_1 < 0$. A further discrimination is thus obtained by ignoring structures for which $\lambda'_1 \geq 0$. The longitudinal direction of the ridge is given by $\mathbf{v}'_2$, the eigenvector corresponding to λ'_2, the modified eigenvalue with smallest magnitude. This provides additional information that can be exploited when linking adjacent ridge pixels, as described next.

3 Tracing Approach

For the linking of adjacent ridge pixels we have adopted the live-wire segmentation paradigm [14–17], which consists in the selection of a starting point by the user followed by the application of a graph-searching algorithm to find the "shortest paths" from that point to all other points in the image according to a predefined cost function. Once computed and stored, the paths can be displayed in real time as the user moves the cursor, allowing for the selection of the next point along the path of interest.

A key component of this approach is the function employed to assign costs to pixels and nearest-neighbor directions. So far, live-wire techniques have been used mainly for the extraction of object contours, with cost functions based on edge descriptors. In order to make the technique suitable for tracing of elongated image structures, we have developed a new cost function based on the ridge detector introduced in the previous section.

Let $\lambda = \lambda'_1$ and $\mathbf{v} = \mathbf{v}'_2$. The cost of linking any pixel $\mathbf{p}$ to an eight-connected neighboring pixel $\mathbf{q}$ in the image is computed in our algorithm as

$$\mathrm{C}(\mathbf{p}, \mathbf{q}) = \gamma \mathrm{C}_\lambda(\mathbf{q}) + (1 - \gamma)\mathrm{C}_\mathbf{v}(\mathbf{p}, \mathbf{q}), \tag{5}$$

where $\gamma \in [0, 1]$ is a user-defined parameter determining

the relative weight of the two normalized cost components, C_λ and $\mathrm{C}_\mathbf{v}$. The former of these is computed from the eigenvalues at $\mathbf{q}$ as

$$\mathrm{C}_\lambda(\mathbf{q}) = 1 - \rho(\mathbf{q}), \tag{6}$$

with

$$\rho(\mathbf{q}) = \begin{cases} \lambda(\mathbf{q})/\lambda_{\min} & \text{if} \quad \lambda(\mathbf{q}) < 0, \\ 0 & \text{if} \quad \lambda(\mathbf{q}) \geq 0, \end{cases} \tag{7}$$

where $\lambda_{\min}$ denotes the smallest λ over all pixels, which in practice will always be less than zero. The second component is computed from the eigenvectors at $\mathbf{p}$ and $\mathbf{q}$ as

$$\mathrm{C}_\mathbf{v}(\mathbf{p},\mathbf{q}) = \tfrac{1}{2}\left\{\sqrt{1-\varphi(\mathbf{p},\mathbf{q})} + \sqrt{1-\varphi(\mathbf{q},\mathbf{p})}\right\}, \tag{8}$$

with

$$\varphi(\mathbf{p},\mathbf{q}) = |\mathbf{w}(\mathbf{p}) \cdot \mathbf{d}(\mathbf{p},\mathbf{q})|, \tag{9}$$

where $\mathbf{w}(\mathbf{p}) = \mathbf{v}(\mathbf{p})/\|\mathbf{v}(\mathbf{p})\|$ is the normalized eigenvector at $\mathbf{p}$, and $\mathbf{d}(\mathbf{p},\mathbf{q}) = (\mathbf{q}-\mathbf{p})/\|\mathbf{q}-\mathbf{p}\|$ the unit "link vector" from $\mathbf{p}$ to $\mathbf{q}$. Note that (8) shows a similar nonlinearity with respect to the inner products as earlier proposed functions [14, 15], but is considerably less computationally expensive due to the absence of trigonometric functions. Also note that since we are taking the absolute value of inner products, the outcome is invariant under vector reversion. Example results with our ridge strength and direction measures ρ and $\mathbf{w}$ are given in Figures 2 and 3.

The graph-searching technique used is an implementation of Dijkstra's shortest-path algorithm based on a discretization of cost values and the use of a circular priority queue [14, 15, 17]. Accurate placing of starting points is facilitated by applying "local snapping": the point indicated by the user is moved to the locally lowest cost point in a small window around that point. The smoothness of the paths computed by the algorithm is improved by applying uniform postfiltering to the coordinates of the path vertices. In cases where the user is not completely satisfied with the paths presented, which might occur in regions with very low contrast-to-noise ratios, we provide the possibility of switching to manual delineation.

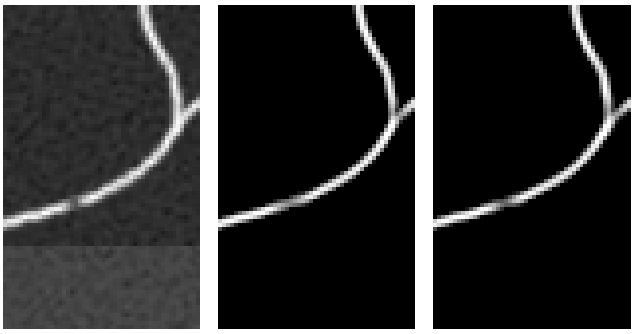

Figure 2. Example of ridge detection using the described filters. Left: a neurite with a small gap, superimposed on a background with noise characteristics and intensity variations as in real fluorescence microscopy images. Middle: the ridgeness ρ as computed from $\mathbf{H}'_{f*G}$. Right: ρ from $\mathbf{H}_{f*G}$. Note that the proposed filter is somewhat better at bridging the gap. Also note the suitability of using a second-order operator: background variations are suppressed without resulting in notable edge responses.

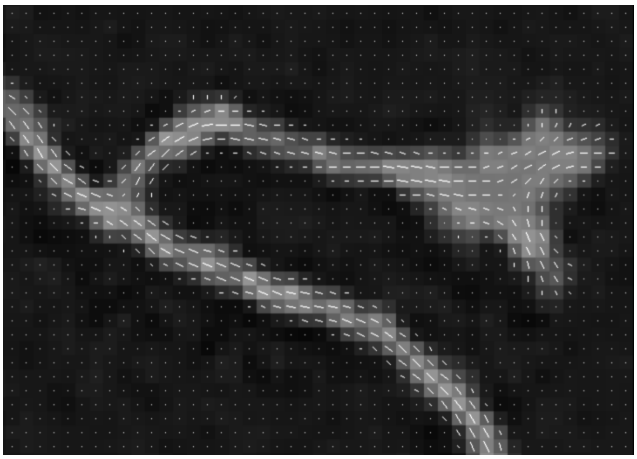

Figure 3. Example of the vector field $\mathbf{w}$ (superimposed white dashes), which we have modulated here by ρ to suppress the vectors in the background.

4 Experimental Results

The described technique was implemented in the Java™ programming language [19] in the form of a plugin for use with ImageJ [20]. After initial experimentation the parameters were fixed to $\gamma = 0.7$ (giving somewhat more weight to the eigenvalue-based cost component), $\sigma = 2.0$ pixels (reflecting the average diameter of neurites in the images), a snap-window size of 9×9 pixels, and a half-window size of 5 vertices for uniform path smoothing. The time required for the precomputation of cost values and, after each mouse click, the recomputation of shortest paths is, of course, dependent on image size and processing platform. On our 2.4GHz Pentium IV computer, both are in the order of 1 second for an image of size 800×800 pixels.

To date, the technique has been applied successfully by biologists in our departments to several hundreds of real fluorescence microscopy images. Based on their experiences we conclude that the proposed approach is a major improvement in speed, accuracy, and reproducibility over currently used, fully manual tracing tools. Two representative example results of tracing using our technique are presented in Figures 4 and 5, which give a visual impression of the accuracy and robustness against noise and intensity discontinuities. We note that obtaining these results required about 25 mouse clicks in both cases. Taking into account the total number of about 15 start, end, and branch points in both cases, which require a mouse click anyway, this is

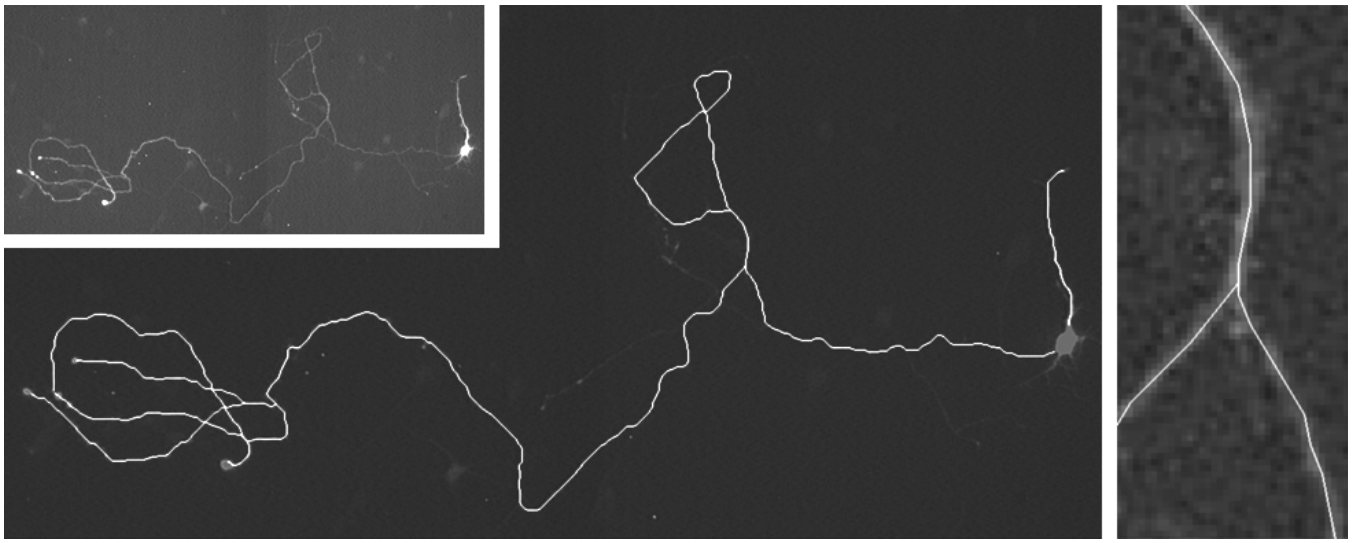

Figure 4. First example of neurite tracing using the described technique. Top-left inset: original fluorescence microscopy image of size 1070×511 pixels showing a cell body (middle-right spot) and its outgrowth. Middle: a low-brightness version of the same image with the tracing result (white curves) superimposed. Right: zoom of a region nearby the center of the image showing how well the tracings follow the neurite centerlines.

not too much. It will be clear that fully manual delineation of all the wiggles with similar precision would require considerably more time and effort.

5 Discussion

In this paper we have presented a live-wire based segmentation technique for the tracing of elongated image structures and have demonstrated its potential for the semiautomatic delineation of neurites in fluorescence microscopy images. The technique is computationally inexpensive and exploits the expertise of the user in solving ambiguities. The underlying algorithm contains surprisingly few parameters, which we have found may easily be kept fixed, yet is very robust. The results of a preliminary evaluation by expert biologists are promising.

We are currently undertaking a more elaborate, quantitative validation study, which should reveal the precise gain in terms of interaction, accuracy, and reduced intra- and inter-observer variability of the described semiautomatic tracing technique compared to currently employed fully manual delineation approaches. To this end the technique has been worked into a full-fledged software tool, which allows the user also to perform measurements and statistical analyses. The tool will be made freely available on the internet upon publication of our results.

References

[1] N. Merlet and J. Zerubia, New prospects in line detection by dynamic programming, *IEEE Trans. Pattern Anal. Machine Intell.*, 18(4), 1996, 426–431.

[2] Y. A. Tolias and S. M. Panas, A fuzzy vessel tracking algorithm for retinal images based on fuzzy clustering, *IEEE Trans. Med. Imaging*, 17(2), 1998, 263–273.

[3] A. F. Frangi, W. J. Niessen, R. M. Hoogeveen, T. van Walsum, and M. A. Viergever, Model-based quantitation of 3-D magnetic resonance angiographic images, *IEEE Trans. Med. Imaging*, 18(10), 1999, 946–956.

[4] O. Wink, A. F. Frangi, B. Verdonck, M. A. Viergever, and W. J. Niessen, 3D MRA coronary axis determination using a minimum cost path approach, *Magn. Res. Med.*, 47(6), 2002, 1169–1175.

[5] Y. Sato, S. Nakajima, N. Shiraga, H. Atsumi, S. Yoshida, T. Koller, G. Gerig, and R. Kikinis, Three-dimensional multi-scale line filter for segmentation and visualization of curvilinear structures in medical images, *Med. Image Anal.*, 2(2), 1998, 143–168.

[6] S. R. Aylward and E. Bullitt, Initialization, noise, singularities, and scale in height ridge traversal for tubular object centerline extraction, *IEEE Trans. Med. Imaging*, 21(2), 2002, 61–75.

[7] F. K. H. Quek and C. Kirbas, Vessel extraction in medical images by wave-propagation and traceback, *IEEE Trans. Med. Imaging*, 20(2), 2001, 117–131.

[8] K. A. Al-Kofahi, S. Lasek, D. H. Szarowski, C. J. Pace, G. Nagy, J. N. Turner, and B. Roysam, Rapid automated three-dimensional tracing of neurons from confocal image stacks, *IEEE Trans. Inf. Technol. Biomed.*, 6(2), 2002, 171–187.

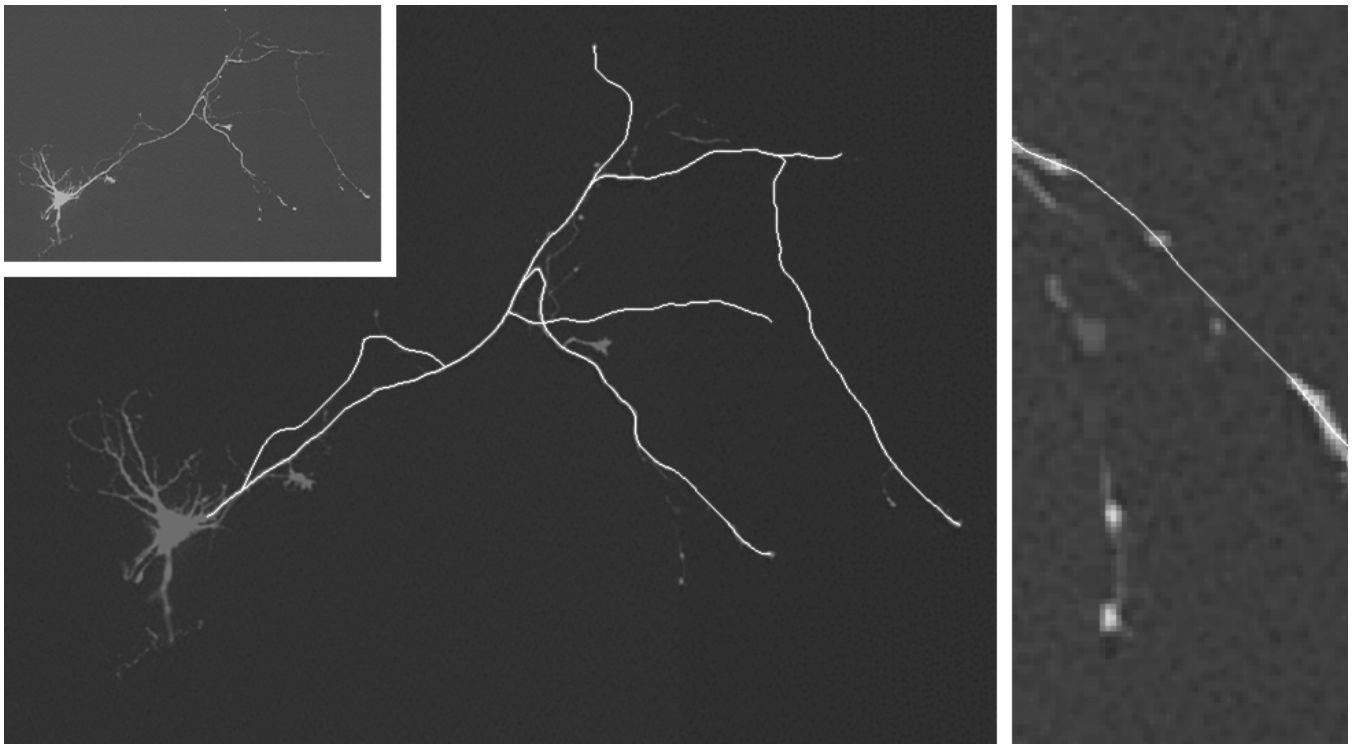

Figure 5. Second example of neurite tracing using the described technique. Top-left inset: original fluorescence microscopy image of size 724×538 pixels showing a cell body (bottom-left spot) and its outgrowth. Middle: a low-brightness version of the same image with the tracing result (white curves) superimposed. Right: zoom of a region towards the bottom-right part of the image, illustrating the robustness of the technique against gross intensity discontinuities.

[9] A. Dima, M. Scholz, and K. Obermayer, Automatic segmentation and skeletonization of neurons from confocal microscopy images based on the 3-D wavelet transform, *IEEE Trans. Image Process.*, 11(7), 2002, 790–801.

[10] J. Teng, Y. Takei, A. Harada, T. Nakata, J. Chen, and N. Hirokawa, Synergistic effects of MAP2 and MAP1B knockout in neuronal migration, dendritic outgrowth, and microtubule organization, *J. Cell Biol.*, 155(1), 2001, 65–76.

[11] T. GrandPré, S. Li, and S. M. Strittmatter, Nogo-66 receptor antagonist peptide promotes axonal regeneration, *Nature*, 417(6888), 2002, 547–551.

[12] I.-J. Kim, H. N. Beck, P. J. Lein, and D. Higgins, Interferon γ induces retrograde dendritic retraction and inhibits synapse formation, *J. Neuroscience*, 22(11), 2002, 4530–4539.

[13] P. Steiner, J. C. F. Sarria, B. Huni, R. Marsault, S. Catsicas, and H. Hirling, Overexpression of neuronal sec1 enhances axonal branching in hippocampal neurons, *Neuroscience*, 113(4), 2002, 893–905.

[14] W. A. Barrett and E. N. Mortensen, Interactive live-wire boundary extraction, *Med. Image Anal.*, 1(4), 1996/7, 331–341.

[15] E. N. Mortensen and W. A. Barrett, Interactive segmentation with intelligent scissors, *Graph. Models Image Process.*, 60(5), 1998, 349–384.

[16] A. X. Falcão, J. K. Udupa, S. Samarasekera, and S. Sharma, User-steered image segmentation paradigms: Live wire and live lane, *Graph. Models Image Process.*, 60(4), 1998, 233–260.

[17] A. X. Falcão, J. K. Udupa, and F. K. Miyazawa, An ultra-fast user-steered image segmentation paradigm: Live wire on the fly, *IEEE Trans. Med. Imaging*, 19(1), 2000, 55–62.

[18] W. T. Freeman and E. H. Adelson, The design and use of steerable filters, *IEEE Trans. Pattern Anal. Machine Intell.*, 13(9), 1991, 891–906.

[19] Sun Microsystems, Inc., Java™ 2 Platform Standard Edition, http://java.sun.com/.

[20] W. Rasband, ImageJ: Image Processing and Analysis in Java, U. S. National Institutes of Health, http://rsb.info.nih.gov/ij/.